Chapter

Water Remediation by G-/GO-Based Photocatalysts

Humaira Seema

Abstract

Graphene, a two-dimensional sheet of sp^2 hybridized carbon atoms, has shown to be the most fascinating and promising option among nanomaterials for a variety of applications, because of its unique structure and tunable physiochemical properties. It can be either in the pure form or in its modified derivatives that include graphene oxide (GO), reduced graphene oxide (rGO), graphene-metal nanoparticle composites, graphene-polymer hybrids, and graphene/organic structures that showed improved results while maintaining inherent properties of the material. These modified nanostructures have a variety of applications as catalysts, energy storage/conversion, antimicrobial, and water decontaminant. In the field of environmental science, graphene has been widely used for molecular sieving involving gas phase separation and organic waste removal from water, due to its biocompatibility, various functional groups, and accessible surface area. Modified graphene can also serve as a semiconductor that can increase the efficiency of the photocatalytic ecosystems that results in the inactivation of the microorganisms causing the organic chemicals to degrade.

Keywords: graphene, environmental, remediation, photocatalyst, water

1. Introduction

Recently photocatalysis by using semiconductors has fascinated universal consideration for its energy-related and environmental applications. Nevertheless, the decrease in the efficiency of the photocatalysis restricted its practical applications because of the prompt reunion of photogenerated electrons and holes. Thus, to decrease the reunion of charge carriers is significant for improvement of semiconductor photocatalysis. Among numerous approaches, water remediation has been done by rGO-/GO-based materials which are the most favorable candidates due to their high capacity of dye adsorption, prolonged light absorption range, improved separation of charge carriers, and transportation properties leading to improved photoconversion efficiency of the photocatalytic materials [1–74].

1.1 Graphene (rGO)-based photocatalysts

Various numbers of graphene-based photocatalysts have been prepared with its derivatives which mainly comprise metal oxides (e.g., P25 [1, 8], TiO_2 [9–34, 36, 37], ZnO [17, 39–43], CuO [44], SnO_2 [13, 45], WO_3 [46]), metals (e.g., Cu [51], Au [52]), metal-metal oxides (e.g., Ag-TiO_2 [35]), upconversion material—P25 (e.g., YF_3:Yb^{3+},Tm^{3+}—TiO_2 [38]), salts (e.g., CdS [47–49], ZnS [50], $ZnFe_2O_4$ [53],

$MnFe_2O_4$ [54], $NiFe_2O_4$ [55], $CoFe_2O_4$ [56], Bi_2WO_6 [57–59], Bi_2MoO_6 [60], $InNbO_4$ [61], ZnSe [63]), Ag/AgCl [62]), and other carbon material (e.g., CNT [64]).

1.2 Graphene oxide (GO)-based photocatalysts

Graphene oxide (GO) has recently received considerable attention due to oxygen-containing functional groups which increase its solubility in solvents for the preparation of GO-based nanocomposites required for photodegradation of pollutants [65–74]. GO-based nanocomposites mainly include metal oxides (TiO_2) [66–72], metal-free polymers [73], and silver/silver halides [74].

2. Preparation of rGO-/GO-based composite photocatalysts

Some of the commonly used synthesis techniques include in situ growth strategy, solution mixing, hydrothermal/ solvothermal, and microwave-assisted process.

2.1 In situ growth strategy

This method is usually used to prepare reduced graphene oxide-/graphene oxide-based metal composites. Zhang et al. reported that TiO_2/graphene composite photocatalyst [14] is synthesized by a simple liquid-phase deposition technique. Moreover, adopting a similar approach, Wang et al. prepared nanocarbon/TiO_2 nanocomposites where titania nanoparticles were decorated by thermal reaction on the surfaces of three different dimensional nanocarbons [9]. While in thermal reduction method, TiO_2/graphene composite [12] with a remarkable visible light photocatalytic activity was prepared by Zhang et al. using a heat treatment method of GO, where GO changed to reduced graphene oxide. Uniform ZnO nanoparticles were found on functionalized graphene sheets evenly via thermal decay of mixture of zinc salt, graphene oxide, and poly(vinyl pyrrolidone) [39].

Furthermore, Sn^{2+} or Ti^{3+} ions were converted to oxides at low temperatures, while GO was reduced to reduced graphene oxide by tin or titanium salts in redox method [13–45]. In our recent work, we prepared SnO_2-G nanocomposite which displayed higher photocatalytic activity in sunlight as compared to bare metal oxide nanoparticles as shown in **Figure 1** [45]. Similarly reduced graphene oxide-zinc oxide composite was prepared where zinc ions were decorated on GO sheets and transformed to metal oxide nanoparticles by using chemical reagents at 150°C. Reduced graphene oxide-ZnO photocatalyst is formed by reducing the graphene oxide [43].

Li et al. prepared uniform mesoporous titania nanospheres on reduced graphene oxide layers via a process of a template-free self-assembly [20]. Du et al. [21] also developed the macro-mesoporous titania-reduced graphene oxide composite film by a confinement of a self-assembly process as shown in **Figure 2**.

Moreover Kim et al. synthesized strongly coupled nanocomposites of layered titanate and graphene by electrostatically derived self-assembly between negatively charged G nanosheets and positively charged TiO_2 nanosols, followed by a phase transition of the anatase TiO_2 component into layered titanate [37]. Chen et al. prepared graphene oxide/titania composites by using the self-assembly technique [72].

While Cu ion-modified reduced graphene oxide [51] prepared by an immersion technique displayed a high photocatalytic activity, gold nanoparticles were decorated on the surface of the reduced graphene oxide through spontaneous chemical reduction of $HAuCl_4$ by GOR [52] as shown in **Figure 3**.

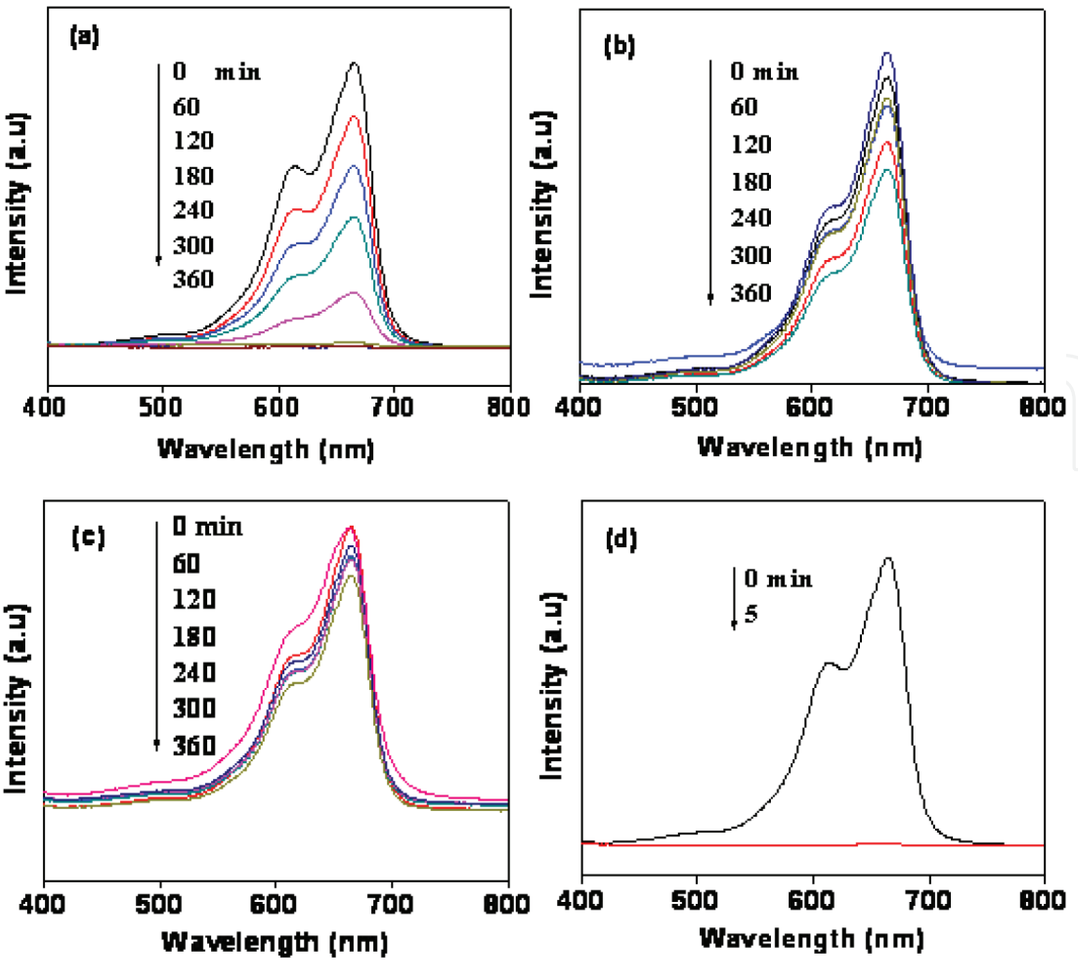

Figure 1.
Time-dependent absorption spectra of MB solution during UV light irradiation in the presence of (a) SnO_2 and (b) reduced graphene oxide-SnO_2 and during sunlight irradiation in the presence of (c) SnO_2 and (d) reduced graphene oxide-SnO_2. Reprinted with permission of the publisher [45].

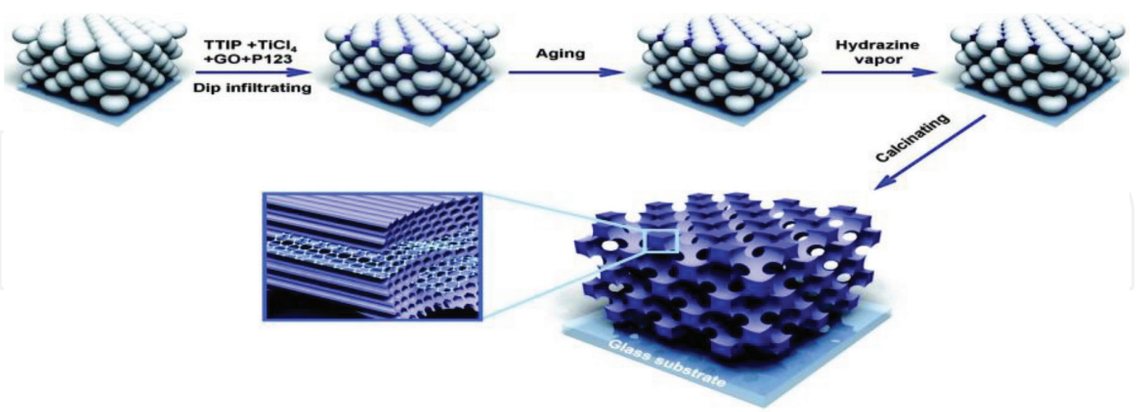

Figure 2.
Schematic view for the preparation of a macro-mesoporous TiO_2-reduced graphene oxide composite film. Reprinted with permission of the publisher [21].

Bi_2WO_6/reduced graphene oxide photocatalysts were successfully prepared via in situ refluxing method in the presence of GO [57]. Zhang et al. presented reduced graphene oxide sheet grafted Ag@AgCl plasmonic photocatalyst with high activity via a precipitation reaction followed by reduction [62]. TiO_2-GO was well prepared at 80°C by using GO and titanium sulfate as precursors [66].

Liu et al. have established a process of water/toluene two-phase for self-assembling TiO_2 nanorods on graphene oxide [69, 70]. Jiang et al. prepared GO/titania

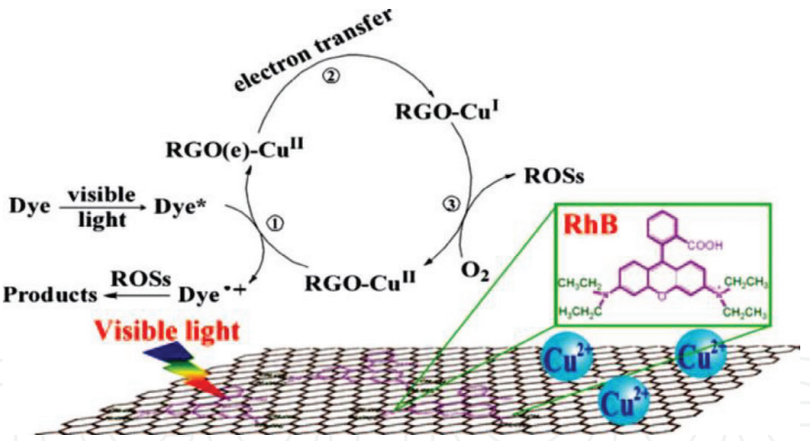

Figure 3.
Possible mechanism of photosensitized degradation of dyes over a rGO Cu composite under visible light irradiation. Reprinted with permission of the publisher [52].

composite by in situ depositing titania on GO through liquid-phase deposition, followed by a calcination at 200°C [71].

GO nanostructures are prepared by modified Hummer's method, which has promising applications in photocatalysis [65].

2.2 Solution mixing method

It has been widely used to prepare graphene-based photocatalysts. Previously, titania nanoparticles and GO colloids have been mixed by ultrasonication followed by ultraviolet (UV)-assisted photocatalytic reduction of GO to yield graphene-titania nanocomposites [18, 23, 31].

Akhavan and Ghaderi used a similar strategy to prepare the titania/reduced graphene oxide composite thin film [25].

Guo et al. [28] prepared TiO_2/graphene composite via sonochemical method. GO/g-C_3N_4 with efficient photocatalytic capability was also fabricated by the same sonochemical approach [73].

ZnO and GO mixture was dispersed by ultrasonication followed by chemical reduction of GO to graphene ultimately leading to synthesize ZnO/graphene composite [40]. The G-hierarchical ZnO hollow sphere composites are synthesized by Luo et al. by using a simple ultrasonic treatment of the solution [43].

Cheng et al. [40] presented a new facile ultrasonic approach to prepare graphene quantum dots (GQDs), which exhibited photoluminescent in a water solution. The water/oil system is used by Zhu et al. [74] to produce graphene oxide enwrapped Ag/AgX (X = Br, Cl) composites. Graphene oxide and silver nitrate solution were added to chloroform solution of surfactants stirring condition at room temperature to produce hybrid composites which displayed high photocatalytic activity under visible light irradiation as shown in **Figure 4**. Titania/graphene oxide composites were synthesized using one-step colloidal blending method [68].

2.3 Hydrothermal/solvothermal method

This one-pot process can lead to highly crystalline nanostructures, which operates at elevated temperatures in an autoclave to generate high pressure, without calcination, and at the same time GO reduced to rGO. Typically, graphene-based composites, e.g., P25 [1, 8], TiO_2 [15, 16, 24, 29, 30, 32–34], Ag-TiO_2 [35], UC-P25 [38], WO_3 [46], CdS [49], $ZnFe_2O_4$ [53], $MnFe_2O_4$ [54], $NiFe_2O_4$ [55], Bi_2WO_6 [58, 59], Bi_2MoO_6 [60], $InNbO_4$ [61], and ZnSe [63], have been prepared by the

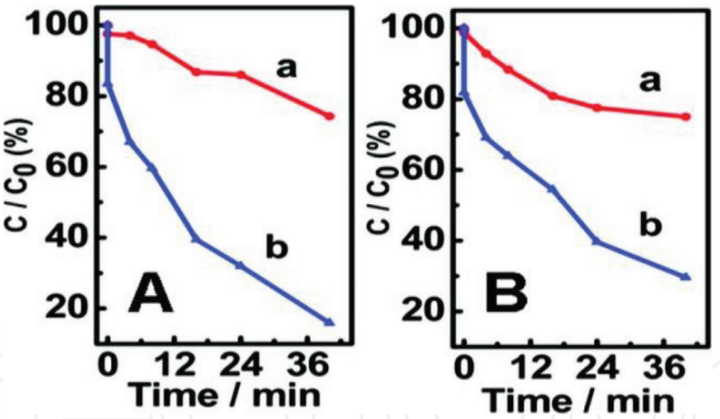

Figure 4.
(A) Photocatalytic activities of silver/silver bromide (a) and silver/silver bromide/GO (b) nanospecies for photodegradation of MO molecules under visible light irradiation and (B) those of the Ag/AgCl (a) and Ag/AgCl/GO (b) nanospecies. Reprinted with permission of the publisher [74].

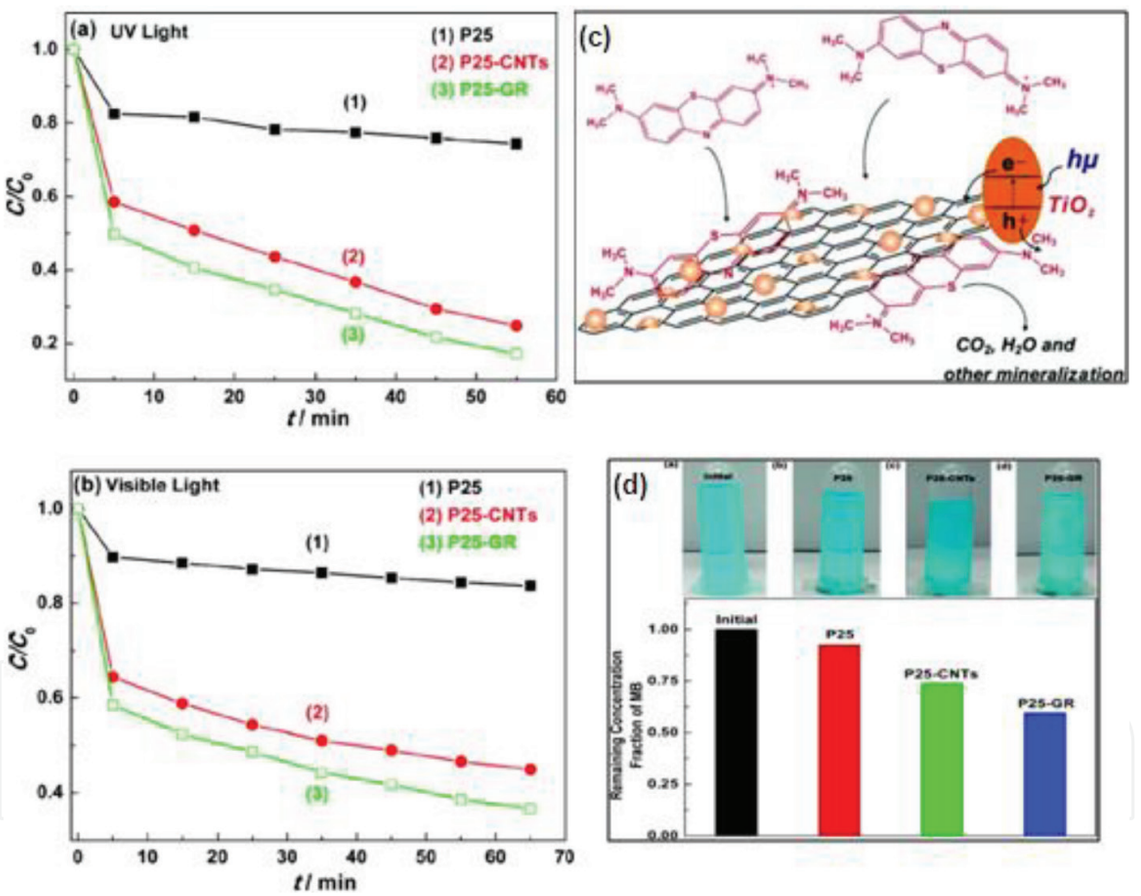

Figure 5.
Photodegradation of MB under (a) UV light (λ = 365 nm) and (b) visible light (λ > 400 nm) over (1) P25, (2) P25-CNTs, and (3) P25-GR photocatalysts, respectively. (c) Schematic structure of P25-GR and process of the photodegradation of MB over P25-GR. (d) Bar plot showing the remaining MB in solution: (1) initial and equilibrated with (2) P25, (3) P25-CNTs, and (4) P25-GR in the dark after 10-min stirring. Pictures of the corresponding dye solutions are on the top for each sample. Reprinted with permission of the publisher [8].

hydrothermal process, while others such as TiO_2 [11, 22, 26, 27], CuO [44], CdS [48], and $CoFe_2O_4$ [56] are prepared by the solvothermal process.

Li et al. have prepared P25-G nanocomposite using GO and P25 as raw materials via hydrothermal technique [8]. As illustrated in **Figure 5**, the photocatalysis determines that composite showed improved activity toward the photodegradation of methylene blue (MB).

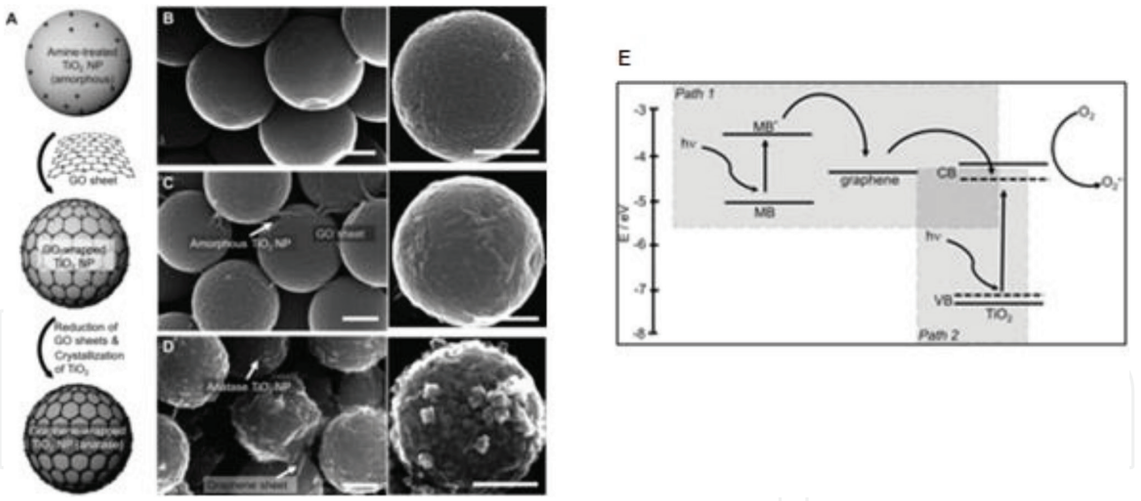

Figure 6.
(A) Schematic illustration of synthesis steps for graphene-wrapped anatase TiO_2 nanoparticles (NPs) and corresponding SEM images of (B) bare amorphous TiO_2 NPs, (C) GO-wrapped amorphous TiO_2 NPs, and (D) graphene-wrapped anatase TiO_2 NPs (scale bar: 200 nm); (E) the suggested mechanism for the photocatalytic degradation of MB by graphene-wrapped anatase TiO_2 NPs under visible light irradiation. Reprinted with permission of the publisher [8].

Lee et al. synthesized graphene oxide (GO)-wrapped TiO_2 nanoparticles by combining positively charged TiO_2 nanoparticles with negatively charged GO nanosheets, as shown in SEM images in **Figure 6**. Furthermore, it demonstrates the reduction of graphene oxide to reduced graphene oxide and the crystallization of amorphous titania nanoparticles which occurred after a hydrothermal treatment.

2.4 Microwave-assisted method

In situ microwave irradiation is a facile method which has been used for the simultaneous formation of metal oxide (e.g., TiO_2 [17], ZnO [17, 41], CdS [47],

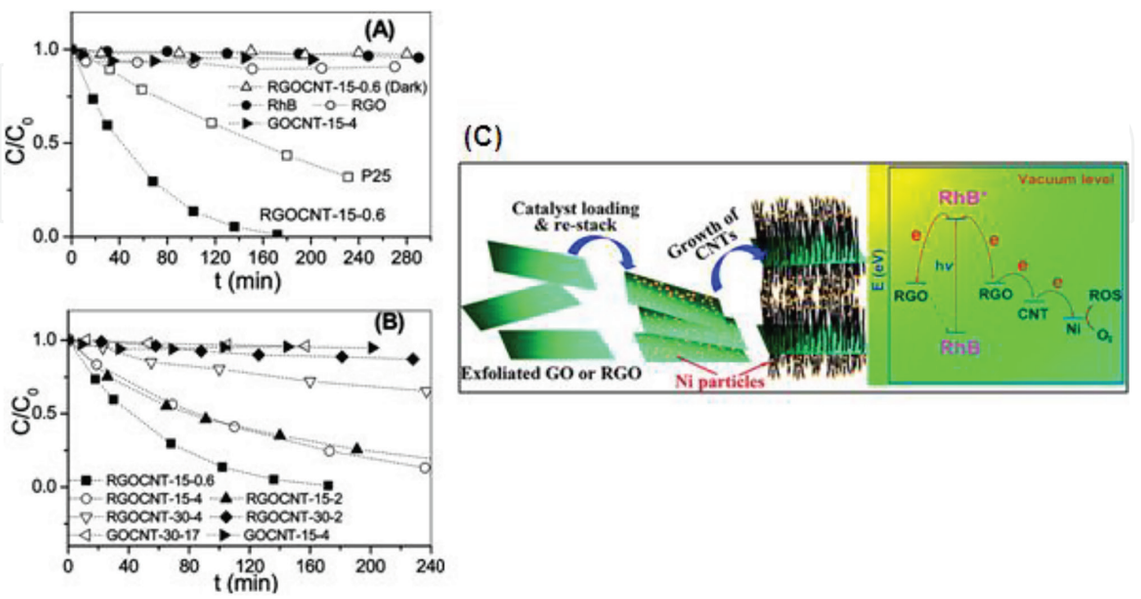

Figure 7.
(A) Photocatalytic degradation for RhB under different experimental conditions with catalysts GOCNT-15-4 and P25. (B) Photocatalytic properties of different samples in degrading RhB. (C) Experimental steps of pillaring GO and RGO platelets with CNTs while energy diagram showing the proposed mechanism of photosensitized degradation of RhB under visible light irradiation. Reprinted with permission of the publisher [64].

ZnS [50]) and reduction of GO. The drawback of this process is that it did not show its fine control over the uniform size and surface distribution of nanoparticles on G surfaces.

2.5 Other methods

In addition to the abovementioned examples, graphene-based photocatalysts are synthesized by developing new synthetic strategies, e.g., electrospinning [10] and chemical vapor deposition (CVD) [64].

Zhao et al. pillared reduced graphene oxide platelets with carbon nanotubes using the CVD method with acetonitrile as the carbon source and nickel nanoparticles as the catalysts as shown in **Figure 7**.

Photocatalytic TiO_2 films were prepared by Yoo et al. using RF magnetron sputtering and GO solutions with different concentrations of GO in ethanol which were coated on TiO_2 films [67]. Graphene film was formed on the surface of TiO_2 nanotube arrays through in situ electrochemical reduction of GO dispersion by cyclic voltammetry [19].

3. Photocatalysis

Due to widespread environmental applications, photocatalysis has fascinated an increasing consideration. The graphene-/graphene oxide-based photocatalyst revealed a significant improvement of photocatalytic degradation of methylene blue (MB) [1, 8, 11, 12, 15, 18, 21, 22, 26, 28, 30–33, 35, 36, 40, 41, 43, 45, 48, 50, 52–56, 60, 61, 67–69], rhodamine B (RhB) [13, 20, 24, 27, 32, 42, 44, 51, 52, 56–59, 62, 64, 73], methyl orange (MO) [9, 10, 14, 37, 38, 49, 63, 66, 71, 72, 74], anthracene-9-carboxylic acid (9-AnCOOH) [19], phenol [22, 54], 2,4-dichlorophenoxyacetic acid (2,4-D) [23], 2,4-dichlorophenol [61, 73], malachite green (MG) [29], 2-propanol [34], rhodamine 6G (Rh 6G) [39], rhodamine B 6G (RhB 6G) [46], orange ll [52], 2,4-dichlorophenol (2,4-DCP) [61], acid orange 7(AO 7) [64], and resazurin (RZ) [65], as well as photocatalytic reduction of Cr(VI) [17, 47, 71], along with photocatalytic antibacterial activity for killing *E. coli* bacteria [25] by UV [1, 8–10, 13, 14, 16–24, 26, 28–34, 37, 39–45, 50, 54, 65–71], as well as visible irradiation [1, 8–13, 15, 16, 20, 22, 25, 27, 30–33, 35–38, 42, 45–49, 51–64, 67, 68, 72–74], in water which are briefly summarized in **Table 1**.

Photocatalysts	Mass fraction	Preparation strategy	Photocatalytic experiments	Performances as compared to reference photocatalyst	Type of irradiation	References
(1) rGO-based						
P25-rGO	0.2% G	Hydrothermal method	Photodegradation of MB	1.17 times higher than P25; DP of 60%	UV	1
	5%			1.50 times		
	30%			0.97 times		
	0.2%			1.42 times higher than P25; DP of 28%	Visible	
	5%			2.32 times		
	30%			0.75 times		
P25-rGO	1.0% G	Hydrothermal method	Photodegradation of MB	3.40 or 1.21 times higher than P25 or P25-CNTs; DP of 25% or 70%, respectively (2% = 90 min)	UV	2

Photocatalysts	Mass fraction	Preparation strategy	Photocatalytic experiments	Performances as compared to reference photocatalyst	Type of irradiation	References
				4.33 or 1.18 times higher than P25 or P25-CNTs; DP of 15% or 55%, respectively (2% = 90 min)	Visible	
TiO_2-rGO	10 mg G	In situ growth strategy (thermal treatment)	Degradation of MO	2.05 times higher than P25; DP of 40%	UV	3
				5.46 times higher than P25; 15%	Visible	
TiO_2-rGO	0.75% G	Electrospin-ning method	Degradation of MO	1.51 times higher than TiO_2; DP of 54%	UV	4
				2.04 times higher than TiO_2; DP of approx. 22%	Visible	
TiO_2-rGO	10 mg G	Solvothermal method	Photodegradation of MB	2.32 or 1.50 times higher than pure TiO_2 or P25; DP of 25% or 39%, respectively	Visible	5
	30 mg			3.0 or 1.92 times		
	50 mg			2.88 or 1.84 times		
TiO_2-rGO	10 mg G	In situ growth strategy (thermal reduction method)	Photodegradation of MB	7.0 times higher than pure P25; DP of 10%	Visible	6
TiO_2-rGO	No data	In situ growth strategy (redox method)	Photodegradation of RhB	1.16 times higher than P25 reaction rate constant = 0.0049 min^{-1}	Visible	7
				0.53 times higher than P25 reaction rate constant = 0.043 min^{-1}	UV	
SnO_2-rGO				2.24 times higher than P25 reaction rate constant = 0.0049 min^{-1}	Visible	
				0.62 times higher than P25 reaction rate constant = 0.043 min^{-1}	UV	
TiO_2-rGO	20 mg G	In situ growth strategy (simple liquid-phase deposition method)	Photodegradation of MO	1.89 times higher than P25 and graphene; DP of 45%	UV	8
TiO_2-rGO	No data	Hydrothermal method	Photodegradation of MB	13.04 or 10.62 times higher than P25 or anatase TiO_2; reaction rate constant = 0.0026 min^{-1} or 0.0032 min^{-1}, respectively	Visible	9
TiO_2-rGO	20: 1	Hydrothermal method	Photodegradation of RhB	1.63 times higher than P25; DP of 52%	UV	10

Photocatalysts	Mass fraction	Preparation strategy	Photocatalytic experiments	Performances as compared to reference photocatalyst	Type of irradiation	References
				3.33 times higher than P25; DP of 15%	Visible	
TiO_2-rGO	0.8% G	Microwave-assisted method	Photocatalytic reduction of Cr(VI)	1.09 or 1.30 times higher than pure TiO_2 or commercial P25 = removal rate of 83% or 70%, respectively	UV	11
rGO-w-TiO_2	1:10	Solution mixing method	Photodegradation of MB	1.25 times higher than P25; DP of 80%	UV	12
TiO_2-rGO film	No data	Cyclic voltammetric reduction method	Photodegradation of anthracene-9-carboxylic acid (9-AnCOOH)	2.13 times higher than bare TiO_2 nanotubes; DP of 46%	UV	13
TiO_2-rGO	6.5% G	In situ growth strategy (self-assembly synthesis)	Photodegradation of RhB	3.92 times higher than TiO_2; DP of 25%	UV-vis	14
TiO_2-rGO	0.6% G	In situ growth strategy (self-assembly method)	Photodegradation of MB	1.57 times higher than TiO_2; reaction rate constant = 0.045 min^{-1}	UV	15
TiO_2-rGO	No data	Solvothermal method	Photodegradation of phenol	1.68 times higher than P25; DP of 48%	UV	16
				3.10 times higher than P25; DP of 20%	Visible	
			Photodegradation of MB	3.5 times higher than P25; DP of 20%	Visible	
TiO_2-rGO film	No data	Solution mixing method	Photodegradation of 2,4-dichlor-ophen-oxyacetic acid (2,4-D)	4.0 times higher than TiO_2 film; reaction rate constant = 0.002 min^{-1}	UV	17
TiO_2-rGO	10% GO	Hydrothermal method	Photodegradation of RhB	4.0 or 2.94 times higher than pure TiO_2 or P25; reaction rate constant = 0.05 or 0.068 min^{-1}	UV	18
TiO_2-rGO	No data	Solution mixing method	Photocatalytic antibacterial activity for killing *E. coli* bacteria	7.55 times higher than TiO_2; reaction rate constant = 0.0086 min^{-1}	Visible	19
TiO_2-rGO	0.3 mg GO	Solvothermal method	Photodegradation of MB	2.08 times higher than P25; DP of 40.8%	UV	20
TiO_2-rGO	No data	Solvothermal method	Photodegradation of RhB	2.79 times higher than P25; reaction rate constant = 0.0162 min^{-1}	Visible	21
TiO_2-rGO	75% G	Sonochemical method	Photodegradation of MB	2.57 times higher than P25; reaction rate constant = 0.0054 min^{-1}	UV	22
TiO_2-rGO	10% G	Hydrothermal method	Photodegradation of Malachite green	3.09 times higher than TiO_2 nanotubes; reaction rate constant = 0.0218 min^{-1}	UV	23

Photocatalysts	Mass fraction	Preparation strategy	Photocatalytic experiments	Performances as compared to reference photocatalyst	Type of irradiation	References
TiO_2-rGO	No data	Hydrothermal method	Photodegradation of MB	1.46 times higher than P25; DP of 65%	UV	24
				2.41 times higher than P25; DP of 29%	Visible	
rGO @TiO_2	1:3	Solution mixing method	Photodegradation of MB	4.0 or 1.73 times higher than P25 or physical mixture of G-P25 (1:3); DP of 13% or 30%, respectively	Visible	25
			Photodegradation of MB	2.93–2.20 times higher than P25 or physical mixture of G-P25 (1:3); DP of 30–40%	UV	
TiO_2-B-doped rGO	2 mg G	Hydrothermal method	Photodegradation of MB	4.30 times higher than TiO_2; reaction rate constant = 0.010 min^{-1}	UV-vis	26
			Photodegradation of RhB	1.6 times higher than TiO_2; reaction rate constant = 0.005 min^{-1}		
TiO_2-N-doped rGO			Photodegradation of MB	2.4 times higher than TiO_2; reaction rate constant = 0.010 min^{-1}		
			Photodegradation of RhB	3.2 times higher than TiO_2; reaction rate constant = 0.005 min^{-1}		
TiO_2-rGO-TiO_2	0.01 g G	Hydrothermal method	Photodegradation of MB	4 times higher than TiO_2	UV-vis	27
TiO_2-rGO/ MCM-41	0.05% G	Hydrothermal method and Thermal method	Photodegradation of 2-propanol	1.4 times higher than TiO_2/MCM-41; conversion rate of 26%	UV	28
	0.15%			1.7 times		
	0.4%			1.27 times		
	0.6%			0.96 times		
Ag-TiO_2-rGO	No data	Hydrothermal and solution mixing method	Photodegradation of MB	Enhancement	Visible	29
RutileTiO_2-GQD/anatase TiO_2-GQD	0.05 g G	Solution mixing method	Degradation of MB	Enhancement for rutile TiO_2/GQD than anatase TiO_2/GQD	Visible	30
Layered titanate rGO	No data	In situ growth strategy (self-assembly method)	Photodegradation of MO	Enhancement as compared to bulk-layered titanates or nanocrystalline-layered titanate	UV-vis	31
UC-P25-rGO UC = YF_3:Yb^{3+},Tm^{3+}	4 mg GO	Hydrothermal method	Photodegradation of MO	2.88 or times higher than P25 or P25-G or UC-P25; DP of 27% or 53% or 46%, respectively	Visible	32
ZnO-rGO	0.6% G	Microwave-assisted method	Photocatalytic reduction of Cr(VI)	1.12 or 0.92 times higher than pure ZnO or P25; removal rate of 58 or 70%, respectively	UV	33

Photocatalysts	Mass fraction	Preparation strategy	Photocatalytic experiments	Performances as compared to reference photocatalyst	Type of irradiation	References
	0.8% G			1.46 or 1.21 times		
	1.0% G			1.68 or 1.40 times		
ZnO-FGS	0.1 g GO	In situ growth strategy (thermal method)	Photodegradation of Rh 6G	Enhancement	UV	34
ZnO-rGO	0.1% G	Solution mixing method (sonochemical)	Photodegradation of MB	2.13 times higher than ZnO; reaction rate constant = 0.022 min^{-1}	UV	35
	0.5%			2.54 times		
	1.0%			3.13 times		
	2.0%			4.45 times		
	3.0%			4.13 times		
	5.0%			3.27 times		
ZnO-rGO	1.1% G	Microwave-assisted method	Photodegradation of MB	1.29 times higher than ZnO; DP of 68%	UV	36
ZnO@ rGO		In situ growth strategy (chemical deposition method)	Photodegradation of RhB	1.05 times higher than ZnO; DP of 95%	UV	37
				1.02 times higher than ZnO; DP of 98%	Visible	
ZnO-rGO	3.56% G	Solution mixing method (ultrasonic method)	Photodegradation of MB	2.25 times higher than ZnO; DP of 40%	UV	38
CuO-rGO	No data	Solvothermal method	Photodegradation of RhB in the presence of H_2O_2	2.50 times higher than ZnO; DP of 40%	UV	39
SnO_2-rGO	5% G	In situ growth strategy (redox method)	Photodegradation of MB	0.40 or times higher than SnO_2; DP of 100%	UV	40
				24.86 times higher than SnO_2; DP of 4%	Visible	
WO_3-rGO	3.5% G	Hydrothermal method	Photodegradation of RhB 6G	2.2 or 53 times higher than WO_3 nanorods or WO_3 particles; reaction rate constant = 0.00167or 0.000069 min^{-1}, respectively	Visible	41
CdS-rGO	1.5% G	Microwave-assisted method	Photocatalytic reduction of Cr(VI)	1.16 times higher than CdS = removal rate of 79%	Visible	42
CdS-rGO	5% G	Solvothermal method	Photodegradation of MB	2.5 times higher than CdS; DP of 37.6%	Visible	43
CdS-rGO	0.01:1	Hydrothermal method	Photodegradation of MO	7.86 times higher than CdS; reaction rate constant = 0.0075 min^{-1}	Visible	44

Photocatalysts	Mass fraction	Preparation strategy	Photocatalytic experiments	Performances as compared to reference photocatalyst	Type of irradiation	References
ZnS-rGO	No data	Microwave-assisted method	Photodegradation of MB	4 times higher than P25; DP of 25%	UV	45
Cu-rGO	No data	In situ growth strategy (immersion method)	Photodegradation of RhB	2.94 or 30.61 times higher than P25 or graphene; reaction rate constant = 0.0051 min^{-1} or 0.00049 min^{-1}, respectively	Visible	46
Au-rGO	No data	In situ growth strategy (chemical reduction)	Photodegradation of RhB	1.77 times higher than P25; reaction rate constant = 0.0049 min^{-1}	Visible	47
			Photodegradation of MB	8.36 times		
			Photodegradation of orange II	0.19 times		
$ZnFe_2O_4$-rGO	20% G	Hydrothermal method	Photodegradation of MB in the presence of H_2O_2	4.50 times higher than $ZnFe_2O_4$ (DP of 22% = 90 min)	Visible	48
$MnFe_2O_4$-rGO	30% G	Hydrothermal method	Photodegradation of MB	9.62 times higher than $MnFe_2O_4$; DP of 10%	Visible	49
			Photodegradation of MB	1.33 times higher than $MnFe_2O_4$; DP of 75%	UV	
			Photodegradation of phenol	1.13 times higher than $MnFe_2O_4$; DP of 75%	UV	
$NiFe_2O_4$-rGO	25% G	Hydrothermal method	Photodegradation of MB	Enhancement as compared to $NiFe_2O_4$; reaction rate constant almost zero (no photocatalytic activity)	Visible	50
$CoFe_2O_4$-rGO	No data	Solvothermal method	Photodegradation of RhB and MB	Enhancement	Visible	51
Bi_2WO_6-rGO	1% G	In situ growth strategy (refluxing method)	Photodegradation of RhB	1.30 times higher than Bi_2WO_6; DP of 50%	Visible	52
	2.5%			1.40 times		
	5%			1.80 times		
	10%			1.10 times		
	15%			0.80 times		
Bi_2WO_6-rGO	1% G	Hydrothermal method	Photodegradation of RhB	Enhancement as compared to Bi_2WO_6	Visible	53
Bi_2WO_6-rGO	No data	Hydrothermal method	Photodegradation of RhB	2.04 times higher than Bi_2WO_6; DP of 44% in 4 min	Visible	54
Bi_2MoO_6-rGO	0.5% G	Hydrothermal method	Photodegradation of MB	2.45 times higher than pure Bi_2MoO_6; reaction rate constant 0.0037 min^{-1}	Visible	55
	1%			3.67 times		

Photocatalysts	Mass fraction	Preparation strategy	Photocatalytic experiments	Performances as compared to reference photocatalyst	Type of irradiation	References
$InNbO_4$-rGO	No data	Hydrothermal method	Photodegradation of MB	1.87 times higher than $InNbO_4$; reaction rate constant = 0.0185 min^{-1}	Visible	56
			Photodegra-dation of 2,4-dichloro-phenol	2.10 times higher than $InNbO_4$ reaction rate constant = 0.0256 min^{-1}		
Ag@AgCl-rGO	0.22% G	Solution mixing method	Photodegradation of RhB	3.88 times higher than Ag@AgCl reaction rate constant = 0.060 min^{-1}	Visible	57
	0.44%			4.55 times		
	1.56%			5.1 times		
ZnSe-N-doped rGO	18 mg G	Hydrothermal method	Photodegradation of MO	Enhancement as compared to ZnSe; (no photocatalytic activity)	Visible	58
CNT-rGO	No data	Chemical vapor deposition (CVD) method	Photodegradation of RhB	4.28 times higher than P25; reaction rate constant = 0.0049 min^{-1}	Visible	59
(2) GO-based						
GO	1 mg GO	Solution mixing method (modified Hummers' method)	Photocatalytic reduction of resazurin (RZ)	No data	UV	60
TiO_2-GO	No data	In situ growth strategy	Photodegradation of MO	2.27 times higher than pure P25; DP of 38.4%	UV	61
TiO_2-GO	0.03 mg GO	RF magnetron sputtering followed by coating	Photodegradation of MB	2.5 times higher than TiO_2; DP of 20%	UV	62
				1.75 times	Visible	
TiO_2-GO	1.2% GO	Solution mixing method (simple colloidal blending method)	Photodegradation of MB	4.51 times higher than P25 reaction rate constant = 0.0084 min^{-1}	UV	63
	4.3%			4.98 times		
	8.2%			8.59 times		
	1.2%			1.36 times higher than P25 reaction rate constant = 0.0033 min^{-1}	Visible	
	4.3%			3.03 times		
	8.2%			7.15 times		
TiO_2-GO	50 mg GO	In situ growth strategy	Photodegradation of MB	1.41 times higher than P25; DP of 70%	UV	64
TiO_2-GO	500 mg GO	In situ growth strategy (two phase assembling method)	Photodegradation of acid orange 7 (AO 7)	11.59 times higher than P25 reaction rate constant = 0.0182 min^{-1}	UV	65

Photocatalysts	Mass fraction	Preparation strategy	Photocatalytic experiments	Performances as compared to reference photocatalyst	Type of irradiation	References
TiO_2-GO	No data	In situ growth strategy (thermal treatment method)	Photodegradation of MO	7.44 times higher than P25; reaction rate constant = 0.0426 min^{-1}	UV	66
			Photocatalytic reduction of Cr(VI)	5.44 times higher than P25; conversion rate = 0.0127 min^{-1}		
TiO_2-GO	0.13% C element	In situ growth strategy (self-assembly method)	Photodegradation of MO	1.18 times higher than pure P25; DP of 22%	Visible	67
	0.14%			1.59 times		
	0.25%			1.0 times		
	0.51%			0.82 times		
g-C_3N_4-GO	1 g GO	Solution mixing method (sonochemical method)	Photodegradation of RhB and 2,4-dichloro-phenol	1.90 times higher than g-C_3N_4; DP of 49.5%	Visible	68
Ag/AgCl/GO	No data	Solution mixing method (surfactant-assisted assembly protocol via an oil/water microemulsion)	Photodegradation of MO	2.84 times higher than Ag/AgCl; DP of 25%	Visible	69
Ag/AgBr/GO			Photodegradation of MO	3.40 times higher than Ag/AgBr; DP of 25%	Visible	

Table 1.
Photocatalytic degradation of pollutants.

Author details

Humaira Seema
Institute of Chemical Sciences, University of Peshawer, Pakistan

*Address all correspondence to: hawkkhan2@gmail.com

References

[1] Zhang Y, Tang ZR, Fu X, Xu YJ. TiO_2-graphene nanocomposites for gas-phase photocatalytic degradation of volatile aromatic pollutant: Is TiO_2-graphene truly different from other TiO_2-carbon composite materials? ACS Nano. 2010;**4**:7303-7314

[2] Huang X, Qi X, Boey F, Zhang H. Graphene-based composites. Chemical Society Reviews. 2012;**41**:666-686

[3] Han L, Wang P, Dong S. Progress in graphene-based photoactive nanocomposites as a promising class of photocatalyst. Nanoscale. 2012;**4**:5814-5825

[4] Xiang Q, Yu J, Jaroniec M. Graphene-based semiconductor photocatalysts. Chemical Society Reviews. 2012;**41**:782-796

[5] Zhang N, Zhang Y, Xu YJ. Recent progress on graphene-based photocatalysts: Current status and future perspectives. Nanoscale. 2012;**4**:5792-5813

[6] Le NH, Seema H, Kemp KC, Ahmed N, Tiwari JN, Park S, et al. Solution-processable conductive micro-hydrogels of nanoparticle/graphene platelets produced by reversible self-assembly and aqueous exfoliation. Journal of Materials Chemistry A. 2013;**1**:12900-12908

[7] Kemp KC, Seema H, Saleh M, Le NH, Mahesh K, Chandra V, et al. Environmental applications using graphene composites: Water remediation and gas adsorption. Nanoscale. 2013;**5**:3149-3171

[8] Zhang H, Lv X, Li Y, Wang Y, Li J. P25-graphene composite as a high performance photocatalyst. ACS Nano. 2009;**4**:380-386

[9] Wang F, Zhang K. Physicochemical and photocatalytic activities of self-assembling TiO_2 nanoparticles on nanocarbons surface. Current Applied Physics. 2012;**12**:346-352

[10] Zhu P, Nair AS, Shengjie P, Shengyuan Y, Ramakrishna S. Facile fabrication of TiO_2-graphene composite with enhanced photovoltaic and photocatalytic properties by electrospinning. ACS Applied Materials & Interfaces. 2012;**4**:581-585

[11] Zhou K, Zhu Y, Yang X, Jiang X, Li C. Preparation of graphene-TiO_2 composites with enhanced photocatalytic activity. New Journal of Chemistry. 2011;**35**:353-359

[12] Zhang Y, Pan C. TiO_2/graphene composite from thermal reaction of graphene oxide and its photocatalytic activity in visible light. Journal of Materials Science. 2011;**46**:2622-2626

[13] Zhang J, Xiong Z, Zhao XS. Graphene-metal-oxide composites for the degradation of dyes under visible light irradiation. Journal of Materials Chemistry. 2011;**21**:3634-3640

[14] Zhang H, Xu P, Du G, Chen Z, Oh K, Pan D, et al. A facile one-step synthesis of TiO_2/graphene composites for photodegradation of methyl orange. Nano Research. 2011;**4**:274-283

[15] Lee JS, You KH, Park CB. Highly photoactive, low bandgap TiO_2 nanoparticles wrapped by graphene. Advanced Materials. 2012;**24**:1084-1088

[16] Wang F, Zhang K. Reduced graphene oxide-TiO_2 nanocomposite with high photocatalystic activity for the degradation of rhodamine B. Journal of Molecular Catalysis A: Chemical. 2011;**345**:101-107

[17] Liu X, Pan L, Lv T, Zhu G, Lu T, Sun Z, et al. Microwave-assisted synthesis of TiO_2-reduced graphene

oxide composites for the photocatalytic reduction of Cr (VI). RSC Advances. 2011;**1**:1245-1249

[18] Seema H, Shirinfar B, Shi G, Youn IS, Ahmed N. Facile synthesis of a selective biomolecule chemosensor and fabrication of its highly fluorescent graphene complex. The Journal of Physical Chemistry B. 2017;**121**:5007-5016

[19] Liu C, Teng Y, Liu R, Luo S, Tang Y, Chen L, et al. Fabrication of graphene films on TiO_2 nanotube arrays for photocatalytic application. Carbon. 2011;**49**:5312-5320

[20] Li N, Liu G, Zhen C, Li F, Zhang L, Cheng HM. Battery performance and photocatalytic activity of mesoporous anatase TiO_2 nanospheres/graphene composites by template-free self-assembly. Advanced Functional Materials. 2011;**21**:1717-1722

[21] Du J, Lai X, Yang N, Zhai J, Kisailus D, Su F, et al. Hierarchically ordered macro-mesoporous TiO_2-graphene composite films: Improved mass transfer, reduced charge recombination, and their enhanced photocatalytic activities. ACS Nano. 2010;**5**:590-596

[22] Jiang B, Tian C, Zhou W, Wang J, Xie Y, Pan Q, et al. In situ growth of TiO_2 in interlayers of expanded graphite for the fabrication of TiO_2-graphene with enhanced photocatalytic activity. Chemistry–A European Journal. 2011;**17**:8379-8387

[23] Shirinfar B, Seema H, Ahmed N. Charged probes: Turn-on selective fluorescence for RNA. Organic & Biomolecular Chemistry. 2018;**16**:164-168

[24] Liang Y, Wang H, Casalongue HS, Chen Z, Dai H. TiO_2 nanocrystals grown on graphene as advanced photocatalytic hybrid materials. Nano Research. 2010;**3**:701-705

[25] Akhavan O, Ghaderi E. Photocatalytic reduction of graphene oxide nanosheets on TiO_2 thin film for photoinactivation of bacteria in solar light irradiation. The Journal of Physical Chemistry C. 2009;**113**:20214-20220

[26] Jiang B, Tian C, Pan Q, Jiang Z, Wang JQ, Yan W, et al. Enhanced photocatalytic activity and electron transfer mechanisms of graphene/TiO_2 with exposed {001} facets. The Journal of Physical Chemistry C. 2011;**115**:23718-23725

[27] Sun L, Zhao Z, Zhou Y, Liu L. Anatase TiO_2 nanocrystals with exposed {001} facets on graphene sheets via molecular grafting for enhanced photocatalytic activity. Nanoscale. 2012;**4**:613-620

[28] Guo J, Zhu S, Chen Z, Li Y, Yu Z, Liu Q, et al. Sonochemical synthesis of TiO_2 nanoparticles on graphene for use as photocatalyst. Ultrasonics Sonochemistry. 2011;**18**:1082-1090

[29] Perera SD, Mariano RG, Vu K, Nour N, Seitz O, Chabal Y, et al. Hydrothermal synthesis of graphene-TiO_2 nanotube composites with enhanced photocatalytic activity. ACS Catalysis. 2012;**2**:949-956

[30] Liu B, Huang Y, Wen Y, Du L, Zeng W, Shi Y, et al. Highly dispersive {001} facets-exposed nanocrystalline TiO_2 on high quality graphene as a high performance photocatalyst. Journal of Materials Chemistry. 2012;**22**:7484-7491

[31] Zhao D, Sheng G, Chen C, Wang X. Enhanced photocatalytic degradation of methylene blue under visible irradiation on graphene@ TiO_2 dyade structure. Applied Catalysis B: Environmental. 2012;**111**:303-308

[32] Gopalakrishnan K, Joshi HM, Kumar P, Panchakarla LS, Rao CN. Selectivity in the photocatalytic properties of the composites of TiO_2

nanoparticles with B-and N-doped graphenes. Chemical Physics Letters. 2011;**511**:304-308

[33] Seema H, Kemp KC, Le NH, Park SW, Chandra V, Lee JW, et al. Highly selective CO_2 capture by S-doped microporous carbon materials. Carbon. 2014;**66**:320-326

[34] Kamegawa T, Yamahana D, Yamashita H. Graphene coating of TiO_2 nanoparticles loaded on mesoporous silica for enhancement of photocatalytic activity. The Journal of Physical Chemistry C. 2010;**114**:15049-15053

[35] Wen Y, Ding H, Shan Y. Preparation and visible light photocatalytic activity of Ag/TiO_2/graphene nanocomposite. Nanoscale. 2011;**3**:4411-4417

[36] Zhuo S, Shao M, Lee ST. Upconversion and downconversion fluorescent graphene quantum dots: Ultrasonic preparation and photocatalysis. ACS Nano. 2012;**6**:1059-1064

[37] Kim IY, Lee JM, Kim TW, Kim HN, Kim HI, Choi W, et al. A strong electronic coupling between graphene nanosheets and layered titanate nanoplates: A soft-chemical route to highly porous nanocomposites with improved photocatalytic activity. Small. 2012;**8**:1038-1048

[38] Ren L, Qi X, Liu Y, Huang Z, Wei X, Li J, et al. Upconversion-P25-graphene composite as an advanced sunlight driven photocatalytic hybrid material. Journal of Materials Chemistry. 2012;**22**:11765-11771

[39] Yang Y, Ren L, Zhang C, Huang S, Liu T. Facile fabrication of functionalized graphene sheets (FGS)/ZnO nanocomposites with photocatalytic property. ACS Applied Materials & Interfaces. 2011;**3**:2779-2785

[40] Xu T, Zhang L, Cheng H, Zhu Y. Significantly enhanced photocatalytic performance of ZnO via graphene hybridization and the mechanism study. Applied Catalysis B: Environmental. 2011;**101**:382-387

[41] Lv T, Pan L, Liu X, Lu T, Zhu G, Sun Z. Enhanced photocatalytic degradation of methylene blue by ZnO-reduced graphene oxide composite synthesized via microwave-assisted reaction. Journal of Alloys and Compounds. 2011;**509**:10086-10091

[42] Li B, Cao H. ZnO@ graphene composite with enhanced performance for the removal of dye from water. Journal of Materials Chemistry. 2011;**21**:3346-3349

[43] Luo QP, Yu XY, Lei BX, Chen HY, Kuang DB, Su CY. Reduced graphene oxide-hierarchical ZnO hollow sphere composites with enhanced photocurrent and photocatalytic activity. The Journal of Physical Chemistry C. 2012;**116**:8111-8117

[44] Liu S, Tian J, Wang L, Luo Y, Sun X. One-pot synthesis of CuO nanoflower-decorated reduced graphene oxide and its application to photocatalytic degradation of dyes. Catalysis Science & Technology. 2012;**2**:339-344

[45] Seema H, Kemp KC, Chandra V, Kim KS. Graphene-SnO_2 composites for highly efficient photocatalytic degradation of methylene blue under sunlight. Nanotechnology. 2012;**23**:355705

[46] An X, Jimmy CY, Wang Y, Hu Y, Yu X, Zhang G. WO_3 nanorods/graphene nanocomposites for high-efficiency visible-light-driven photocatalysis and NO_2 gas sensing. Journal of Materials Chemistry. 2012;**22**:8525-8531

[47] Liu X, Pan L, Lv T, Zhu G, Sun Z, Sun C. Microwave-assisted synthesis of CdS-reduced graphene oxide composites for photocatalytic reduction

of Cr (vi). Chemical Communications. 2011;**47**:11984-11986

[48] Wang X, Tian H, Yang Y, Wang H, Wang S, Zheng W, et al. Reduced graphene oxide/CdS for efficiently photocatalytic degradation of methylene blue. Journal of Alloys and Compounds. 2012;**524**:5-12

[49] Ye A, Fan W, Zhang Q, Deng W, Wang Y. CdS–graphene and CdS–CNT nanocomposites as visible-light photocatalysts for hydrogen evolution and organic dye degradation. Catalysis Science & Technology. 2012;**2**:969-978

[50] Hu H, Wang X, Liu F, Wang J, Xu C. Rapid microwave-assisted synthesis of graphene nanosheets–zinc sulfide nanocomposites: Optical and photocatalytic properties. Synthetic Metals. 2011;**161**:404-410

[51] Xiong Z, Zhang LL, Zhao XS. Visible-light-induced dye degradation over copper-modified reduced graphene oxide. Chemistry–A European Journal. 2011;**17**:2428-2434

[52] Xiong Z, Zhang LL, Ma J, Zhao XS. Photocatalytic degradation of dyes over graphene-gold nanocomposites under visible light irradiation. Chemical Communications. 2010;**46**:6099-6101

[53] Fu Y, Wang X. Magnetically separable $ZnFe_2O_4$-graphene catalyst and its high photocatalytic performance under visible light irradiation. Industrial & Engineering Chemistry Research. 2011;**50**:7210-7218

[54] Fu Y, Xiong P, Chen H, Sun X, Wang X. High photocatalytic activity of magnetically separable manganese ferrite-graphene heteroarchitectures. Industrial & Engineering Chemistry Research. 2012;**51**:725-731

[55] Fu Y, Chen H, Sun X, Wang X. Graphene-supported nickel ferrite: A magnetically separable photocatalyst with high activity under visible light. AIChE Journal. 2012;**58**:3298-3305

[56] Min YL, Zhang K, Chen YC, Zhang YG. Enhanced photocatalytic performance of Bi_2WO_6 by graphene supporter as charge transfer channel. Separation and Purification Technology. 2012;**86**:98-105

[57] Zhou F, Shi R, Zhu Y. Significant enhancement of the visible photocatalytic degradation performances of γ-Bi_2MoO_6 nanoplate by graphene hybridization. Journal of Molecular Catalysis A: Chemical. 2011;**340**:77-82

[58] Zhang X, Quan X, Chen S, Yu H. Constructing graphene/$InNbO_4$ composite with excellent adsorptivity and charge separation performance for enhanced visible-light-driven photocatalytic ability. Applied Catalysis B: Environmental. 2011;**105**:237-422

[59] Ying H, Wang ZY, Guo ZD, Shi ZJ, YANG SF. Reduced graphene oxide-modified Bi_2WO_6 as an improved photocatalyst under visible light. Acta Physico-Chimica Sinica. 2011;**27**:1482-1486

[60] Bai S, Shen X, Zhong X, Liu Y, Zhu G, Xu X, et al. One-pot solvothermal preparation of magnetic reduced graphene oxide-ferrite hybrids for organic dye removal. Carbon. 2012;**50**:2337-2346

[61] Gao E, Wang W, Shang M, Xu J. Synthesis and enhanced photocatalytic performance of graphene-Bi_2WO_6 composite. Physical Chemistry Chemical Physics. 2011;**13**:2887-2893

[62] Zhang H, Fan X, Quan X, Chen S, Yu H. Graphene sheets grafted Ag@AgCl hybrid with enhanced plasmonic photocatalytic activity under visible light. Environmental Science & Technology. 2011;**45**:5731-5736

[63] Chen P, Xiao TY, Li HH, Yang JJ, Wang Z, Yao HB, et al. Nitrogen-doped graphene/ZnSe nanocomposites: Hydrothermal synthesis and their enhanced electrochemical and photocatalytic activities. ACS Nano. 2011;**6**:712-719

[64] Zhang LL, Xiong Z, Zhao XS. Pillaring chemically exfoliated graphene oxide with carbon nanotubes for photocatalytic degradation of dyes under visible light irradiation. ACS Nano. 2010;**4**:7030-7036

[65] Krishnamoorthy K, Mohan R, Kim SJ. Graphene oxide as a photocatalytic material. Applied Physics Letters. 2011;**98**:244101

[66] Zhang Q, He Y, Chen X, Hu D, Li L, Yin T, et al. Structure and photocatalytic properties of TiO_2-graphene oxide intercalated composite. Chinese Science Bulletin. 2011;**56**:331-339

[67] Yoo DH, Cuong TV, Pham VH, Chung JS, Khoa NT, Kim EJ, et al. Enhanced photocatalytic activity of graphene oxide decorated on TiO_2 films under UV and visible irradiation. Current Applied Physics. 2011;**11**:805-808

[68] Nguyen-Phan TD, Pham VH, Shin EW, Pham HD, Kim S, Chung JS, et al. The role of graphene oxide content on the adsorption-enhanced photocatalysis of titanium dioxide/graphene oxide composites. Chemical Engineering Journal. 2011;**170**:226-232

[69] Liu J, Bai H, Wang Y, Liu Z, Zhang X, Sun DD. Self-assembling TiO_2 nanorods on large graphene oxide sheets at a two-phase interface and their anti-recombination in photocatalytic applications. Advanced Functional Materials. 2010;**20**:4175-4181

[70] Liu J, Liu L, Bai H, Wang Y, Sun DD. Gram-scale production of graphene oxide-TiO_2 nanorod composites: Towards high-activity photocatalytic materials. Applied Catalysis B: Environmental. 2011;**106**:76-82

[71] Jiang G, Lin Z, Chen C, Zhu L, Chang Q, Wang N, et al. TiO_2 nanoparticles assembled on graphene oxide nanosheets with high photocatalytic activity for removal of pollutants. Carbon. 2011;**49**:2693-2701

[72] Chen C, Cai W, Long M, Zhou B, Wu Y, Wu D, et al. Synthesis of visible-light responsive graphene oxide/TiO_2 composites with p/n heterojunction. ACS Nano. 2010;**4**:6425-6432

[73] Liao G, Chen S, Quan X, Yu H, Zhao H. Graphene oxide modified gC_3N_4 hybrid with enhanced photocatalytic capability under visible light irradiation. Journal of Materials Chemistry. 2012;**22**:2721-2726

[74] Zhu M, Chen P, Liu M. Graphene oxide enwrapped Ag/AgX (X = Br, Cl) nanocomposite as a highly efficient visible-light plasmonic photocatalyst. ACS Nano. 2011;**5**:4529-4536